ELSEVIER

Chemical Engineering Science 61 (2006) 1138–1145

Chemical Engineering Science

www.elsevier.com/locate/ces

Adsorption of zinc(II) from water with purified carbon nanotubes

Chungsying Lu*, Huantsung Chiu

Department of Environmental Engineering, National Chung Hsing University, 250 Kuo Kuang Road, Taichung 402, Taiwan, ROC

Received 29 April 2005; received in revised form 22 July 2005; accepted 6 August 2005
Available online 23 September 2005

Abstract

Commercial single-walled carbon nanotubes (SWCNTs) and multi-walled carbon nanotubes (MWCNTs) were purified by sodium hypochlorite solutions and were employed as adsorbents to study the adsorption characteristics of zinc from water. The properties of CNTs such as purity, structure and nature of the surface were greatly improved after purification which made CNTs become more hydrophilic and suitable for adsorption of Zn^{2+}. In general, the adsorption capacity of Zn^{2+} onto CNTs increased with the increase of pH in the pH range of 1–8, fluctuated very little and reached maximum in the pH range of 8–11 and decreased at a pH of 12. A comparative study on the adsorption of Zn^{2+} between CNTs and commercial powdered activated carbon (PAC) was also conducted. The maximum adsorption capacities of Zn^{2+} calculated by the Langmuir model are 43.66, 32.68, and 13.04 $\mathrm{mg\,g^{-1}}$ with SWCNTs, MWCNTs and PAC, respectively, at an initial Zn^{2+} concentration range of 10–80 $\mathrm{mg\,l^{-1}}$. The short contact time needed to reach equilibrium as well as the high adsorption capacity suggests that SWCNTs and MWCNTs possess highly potential applications for the removal of Zn^{2+} from water.

Keywords: Carbon nanotubes; Adsorption; Zinc; pH effect; Powdered activated carbon

1. Introduction

The presence of heavy metals such as cadmium, copper, lead, nickel, mercury and zinc in aqueous environment may result in a major concern due to their toxicity and carcinogenicity which may cause damage to various systems of the human body (Purdom, 1980). As a result, more stringent requirements for the removal of heavy metals from aqueous environment, in recent years, have necessitated the development of innovative, cost-effective treatment alternatives.

Carbon nanotubes (CNTs) are relatively new adsorbents that have proven very efficient for treating many kinds of trace pollutants such as dioxin from air (Long and Yang, 2001) or lead (Li et al., 2002a), cadmium (Li et al., 2003a), fluoride (Li et al., 2003b), 1,2-dichlorobenzene (Peng et al., 2003) or THMs (Lu et al., 2005) from water. The comparisons of CNTs with other commercial adsorbents made by the foregoing researchers suggest that CNTs have great potential in environmental protection applications. However, the studies on the adsorption of heavy metals with CNTs are still very limited in the literature. This paper aims at investigating adsorption characteristics of zinc, which is commonly discharged from many kinds of industrial activities such as chemicals, metals, pulp and paper manufacturing processes (Eckenfelder, 1989), with CNTs. A comparative study on the adsorption of zinc between CNTs and commercial powdered activated carbon (PAC) is also conducted.

2. Materials and methods

2.1. Preparation of purified CNTs

Multi-walled CNTs with outer diameter (dp) < 10 nm (L-MWCNTs, Nanotech Port Co., Shenzhen, China) and single-walled carbon nanotubes with dp < 2 nm (L-SWCNTs, Nanotech Port Co., Shenzhen, China) were selected as adsorbents to study adsorption characteristics of Zn^{2+} from water. The length of CNTs was in the range of 5–15 μm and the mass ratio of amorphous carbon was less than 5%.

---

* Corresponding author. Tel.: +886 4 22852483; fax: +886 4 22862587.
E-mail address: clu@dragon.nchu.edu.tw (C. Lu).

doi:10.1016/j.ces.2005.08.007

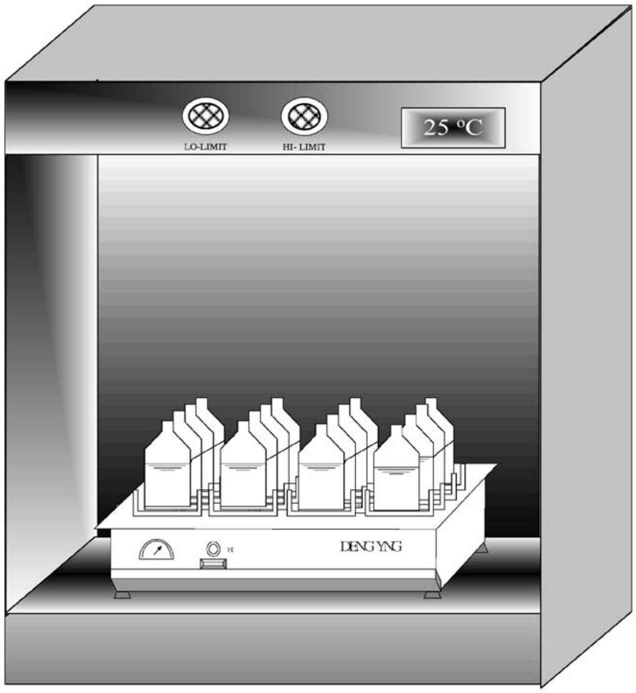

Fig. 1. Experimental setup of the batch system.

Raw CNTs (3 g) were heated at 350 °C for 30 min to remove amorphous carbon. After thermal treatment, half gram of CNTs was dispersed into a flask containing 20 ml of 70% sodium hypochlorite solution (6 ml of H_2O+14 ml of NaClO). The solution was then shaken in an ultrasonic cleaning bath (Model D400H, Delta Instruments Co., USA) for 20 min and was heated at 85 °C in a water bath for 3 h to remove metal catalysts. After cooling, the CNTs were washed with deionized water until the pH of the solution reached 7. Finally, the solution was filtered through a 0.45 μm Nylon fiber filter and purified CNTs were obtained.

2.2. Preparation of Zn^{2+} solution

Analytical-grade zinc nitrate (Merck Ltd., Taipei, Taiwan, 96–97% purity) was employed to prepare a stock solution containing 1000 $\mathrm{mg\,l^{-1}}$ of Zn^{2+}, which was further diluted with deionized water to the desired Zn^{2+} concentrations.

2.3. Batch adsorption experiments

Batch adsorption experiments were performed using 150 ml glass bottles with addition of 50 mg of CNTs and 100 ml of Zn^{2+} solution of increased initial concentrations (C_0) from 10 to 80 $\mathrm{mg\,l^{-1}}$. The glass bottles were sealed with Teflon and then were mounted on a shaker. The shaker was placed within a temperature control box (Model CH-502, Chin Hsin, Taipei, Taiwan) and operated at 25 °C and 180 rpm for 12 h. Fig. 1 shows the experimental setup of the batch system. The pH of the solution was maintained at 7 with the exception of pH effect study, in which the pH range of 1–12 was chosen. The pH was adjusted using 0.1 M HNO_3 or 0.1 M NaOH.

The adsorbed Zn^{2+} was calculated as follows:

$$q = (C_0 - C_t)V/m, \tag{1}$$

where q is the amount of Zn^{2+} adsorbed by CNTs ($\mathrm{mg\,g^{-1}}$); C_0 is the initial Zn^{2+} concentration ($\mathrm{mg\,l^{-1}}$); C_t is the final Zn^{2+} concentration after a certain period of time ($\mathrm{mg\,l^{-1}}$); V is the initial solution volume (l) and m is the CNTs dosage (g).

2.4. Isotherm models

The experimental data for Zn^{2+} adsorption onto CNTs could be approximated by the isotherm models, respectively, of Langmuir and Freundlich:

$$q = \frac{abC_e}{1 + bC_e}, \tag{2}$$

$$q = K_f C_e^n, \tag{3}$$

where C_e is the equilibrium concentration of Zn^{2+} ($\mathrm{mg\,l^{-1}}$); a and b are Langmuir constants and K_f and n are Freundlich constants.

2.5. Analytical methods

The concentration of Zn^{2+} was determined by a flame atomic absorption spectrometer (FAAS, Model 100, Perkin-Elmer, USA). The morphology of CNTs was analyzed by a field emission scanning electron microscope (FE-SEM, JEOL JSM-6700, Tokyo, Japan) and a high-resolution transmission electron microscope (HR-TEM, JEOL JEM-2010, Tokyo, Japan). The structural information of CNTs was evaluated by a Raman Spectrometer (Model Nanofinder 30 R., Tokyo Instruments Inc., Tokyo, Japan). The functional groups on the surface of CNTs were detected by fourier transform infrared spectroscopy (Model FT/IR-200, JAS Co., Tokyo, Japan).

Zeta potentials of the CNTs were measured across the pH range of 2–12. Samples were prepared identically to those of the batch experiments. Measurements were made on a Malvern Zetasizer (Model ZEN 1001, Malvern Instrument Co., UK). Thirty measurements were made for each sample and the average value was taken as the zeta potential of the CNTs under that particular pH condition.

The surface area of CNTs and pore size distribution were calculated from nitrogen adsorption isotherm data (Micromertics ASAP 2010, USA) that were completed with a 0.3138 g sample at 77.48 K using the Brunauer, Emmett and Teller (BET), and Barrett, Johner and Halenda (BJH) methods, respectively.

3. Results and discussion

3.1. Characterization of CNTs

Figs. 2a and b show the SEM images of raw and purified SWCNTs and MWCNTs, respectively. It is evident that the isolated CNTs usually curve and have cylindrical shapes with the diameter range of 1–2 and 8–10 nm for SWCNTs and MWCNTs, respectively. Due to inter-molecular force, the isolated CNTs of different size and direction form an aggregated structure. The length of CNTs becomes short and the confined space among isolated CNTs becomes small after purification.

Figs. 3a and b display the TEM images of raw and purified SWCNTs and MWCNTs, respectively. As can be seen, a large amount of metal catalysts and amorphous carbon appeared within raw CNTs and was removed after purification. TEM images of purified SWCNTs showed large quantities of nanotube bundles with the hollow inner tube diameter of around 1.5 nm. TEM images of MWCNT contained a concentrically nested array of SWCNTs with the hollow inner tube diameter of around 4 nm.

Figs. 4a and b display Raman spectra of raw and purified SWCNTs and MWCNTs, respectively. It is seen that there are two peaks located at around 1350 and 1580 cm^{-1}. The peak near 1350 cm^{-1} is the so-called D band which is related to disordered sp^2-hybridized carbon atoms of nanotubes. The peak near 1580 cm^{-1} is the so-called G band which is related to the graphite E_{2g} symmetry of the interlayer mode. This mode reflects the structural integrity of sp^2-hybridized carbon atoms of the nanotubes. Together, these bands can be used to evaluate the extent of carbon-containing defects (Dresselhaus et al., 2002; Tsai and Chen, 2003; Ko et al., 2004). The intensity ratios of D band to G band (I_D/I_G) of raw and purified CNTs are 0.255 and 0.165 with SWCNTs and are 0.503 and 0.371 with MWCNTs. The I_D/I_G ratios of SWCNTs are lower than those of MWCNTs implying that SWCNTs possess more graphitized structures and better properties. Furthermore, the I_D/I_G ratios of raw CNTs are higher than those of purified CNTs indicating that the surface properties of CNTs were greatly improved after purification by 70% of sodium hypochlorite solution.

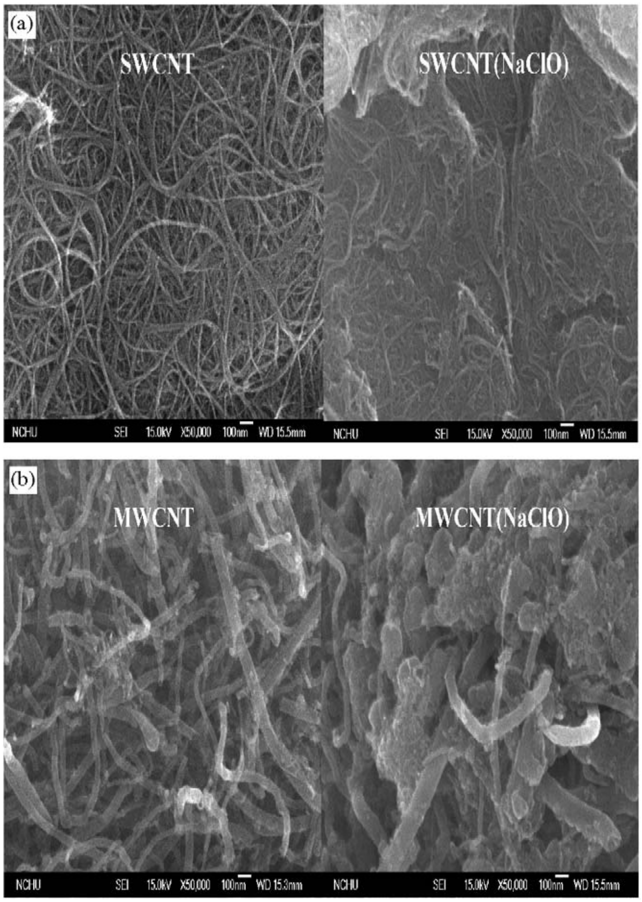

Fig. 2. Scanning electron microscope images of CNTs: (a) SWCNT, (b) MWCNT.

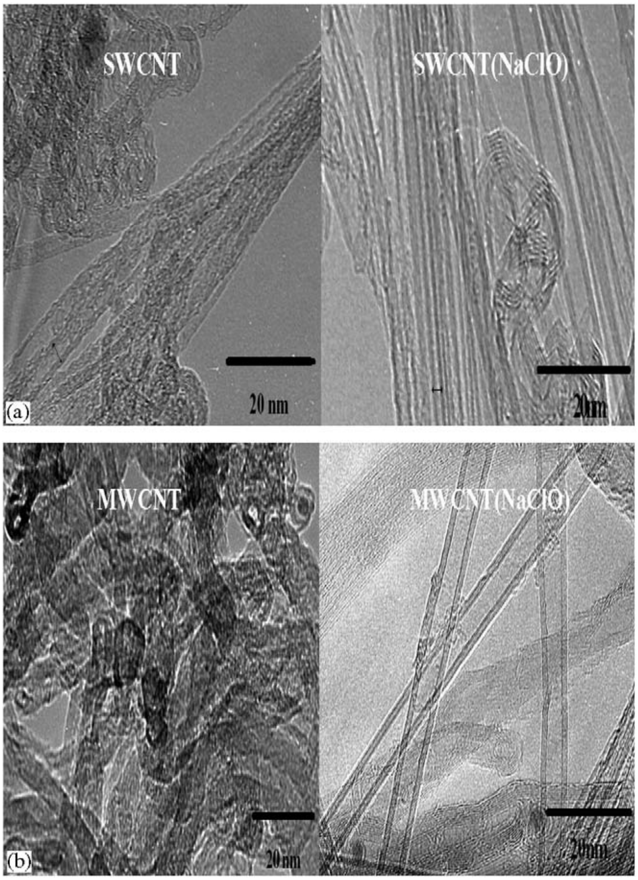

Fig. 3. Transmission electron microscope images of CNTs: (a) SWCNT, (b) MWCNT.

Figs. 5a and b show the Fourier-transformed infrared spectra of raw and purified SWCNTs and MWCNTs, respectively. It is seen that the raw CNTs exhibit insignificant peaks. In contrast, the purified CNTs exhibit three major peaks at wavenumbers near 1400, 1700 and 3500 cm^{-1} which are associated with carboxylic acids and phenolic

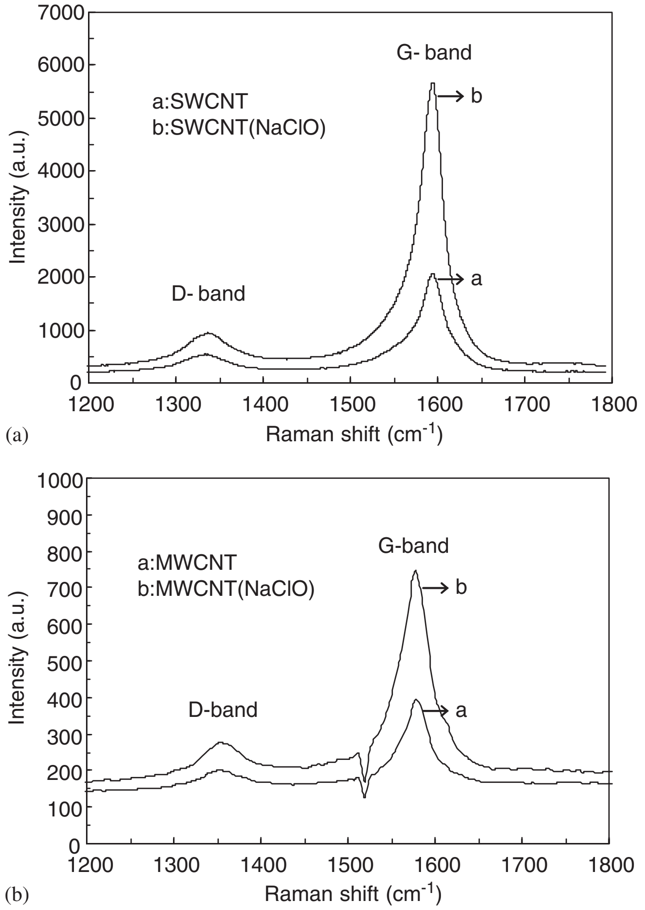

Fig. 4. Raman spectra of CNTs: (a) SWCNT, (b) MWCNT.

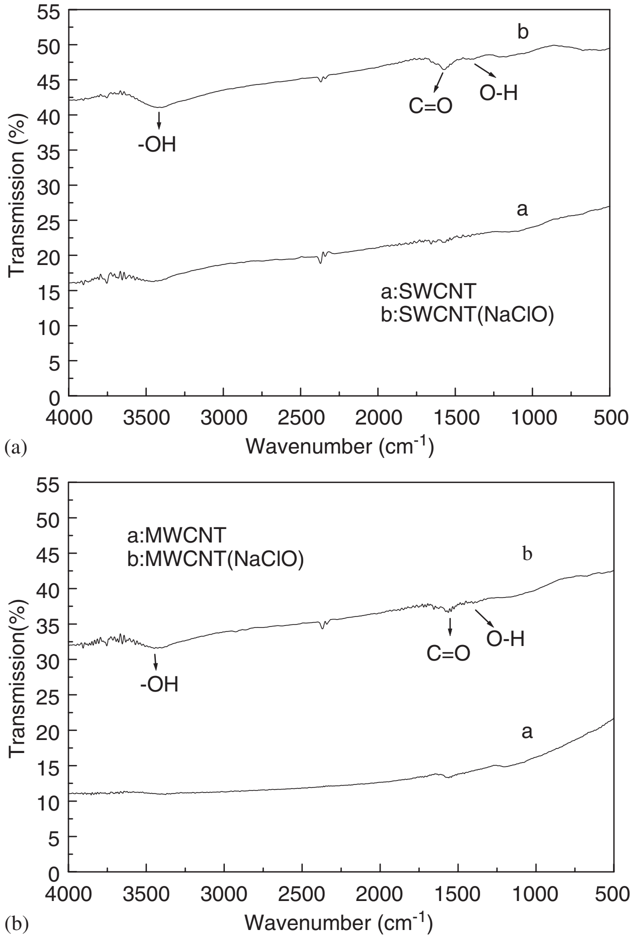

Fig. 5. Pore size distributions of CNTs: (a) SWCNT, (b) MWCNT.

groups (O–H), carbonyl groups (> C=O) and hydroxyl groups (–OH) (Li et al., 2002b; Lu et al., 2005).

Figs. 6a and b exhibit the pore size distribution of raw and purified SWCNTs and MWCNTs, respectively. The peaks of raw and purified SWCNTs are located in the size range of 7–12 and 3–5 nm, respectively. These pores are likely to be contributed by aggregated pores which are formed with the confined space among the isolated SWCNTs (Yang et al., 2001). The low detection limit for pore size of the employed BET analyzer is around 2 nm. Therefore, a quantification of the inner diameter distribution of SWCNTS less than 2 nm is not possible in this study.

The pore size of MWCNTs is a bimodal distribution. The minor peaks of raw and purified MWCNTs are both located in the size range of 3–4 nm while the major peaks are located in the size range of 10–30 and 7–12 nm, respectively. The 3–4 nm pores are the CNT inner cavities, close to the inner diameter of MWCNTs. The 10–30 and 7–12 nm pores are the aggregated pores of raw and purified MWCNTs, respectively.

It is obvious that the pore size range of the major peak of CNTs decreases after purification. This indicates that the confined space of isolated CNTs becomes small after purification. The change in the pore size range of the minor peak of CNTs after purification is insignificant.

The physical properties of raw and purified SWCNTs and MWCNTs measured by a BET analyzer are listed in Table 1. As can be seen, the surface area and pore volume of SWCNTs are higher than those of MWCNTs but the average pore diameter of SWCNTs is lower than that of MWCNTs. The surface area, average pore diameter and pore volume of CNTs decrease after purification. Possible reason may be attributed to the fact that the length of CNTs becomes short and the confined space among isolated CNTs becomes small after purification as indicated in Fig. 2.

Figs. 7a and b show the effect of pH on the zeta potential of raw and purified SWCNTs and MWCNTs, respectively. In both cases the zeta potentials of CNTs become more negative with the increase of pH. The pH value at which the positive surface charge equals the negative surface charge (i.e., iso-electric point) is defined as pH_{iep}. Raw SWCNTs show a pH_{iep} of 4.6 and raw MWCNTs a pH_{iep} of 4.9 indicating that the surface of the raw CNTs maintained acidic characteristics. The zeta potentials of purified CNTs were more negative than those of raw CNTs and were all negative values within the pH range tested herein. This is

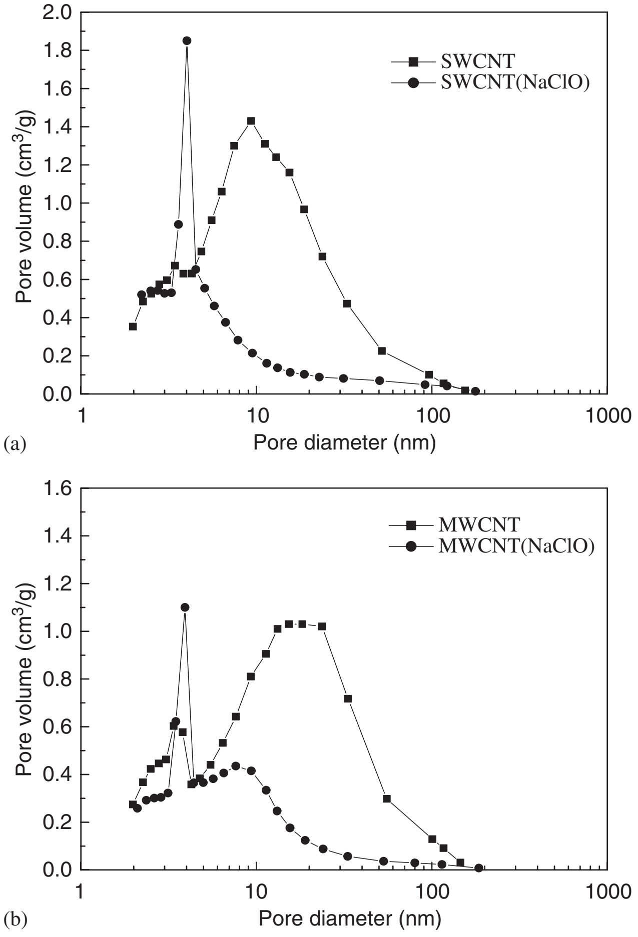

Fig. 6. Fourier transformed infrared spectra of CNTs: (a) SWCNT, (b) MWCNT.

probably due to the presence of negative functional groups on the surface of purified CNTs as shown in Fig. 5. From an electrostatic interaction point of view, adsorption of Zn^{2+} onto purified SWCNTs and MWCNTs is electrostatically attractive for the pH range of 2–12.

3.2. Effect of contact time

Figs. 8a and b show the effect of contact time on the adsorption of Zn^{2+} onto purified SWCNTs and MWCNTs, respectively, for $C_0 = 10$ and $60\,\mathrm{mg\,l^{-1}}$. It is noted that the adsorption of Zn^{2+} increased quickly with time and then reached equilibrium. The contact time to reach equilibrium was 60 min. The final capacities for adsorption of Zn^{2+} onto SWCNTs and MWCNTs reached 14.9 and $13.75\,\mathrm{mg\,g^{-1}}$, respectively, for $C_0 = 10\,\mathrm{mg\,l^{-1}}$ and achieved 35.9 and $28.75\,\mathrm{mg\,g^{-1}}$, respectively, for $C_0 = 60\,\mathrm{mg\,l^{-1}}$.

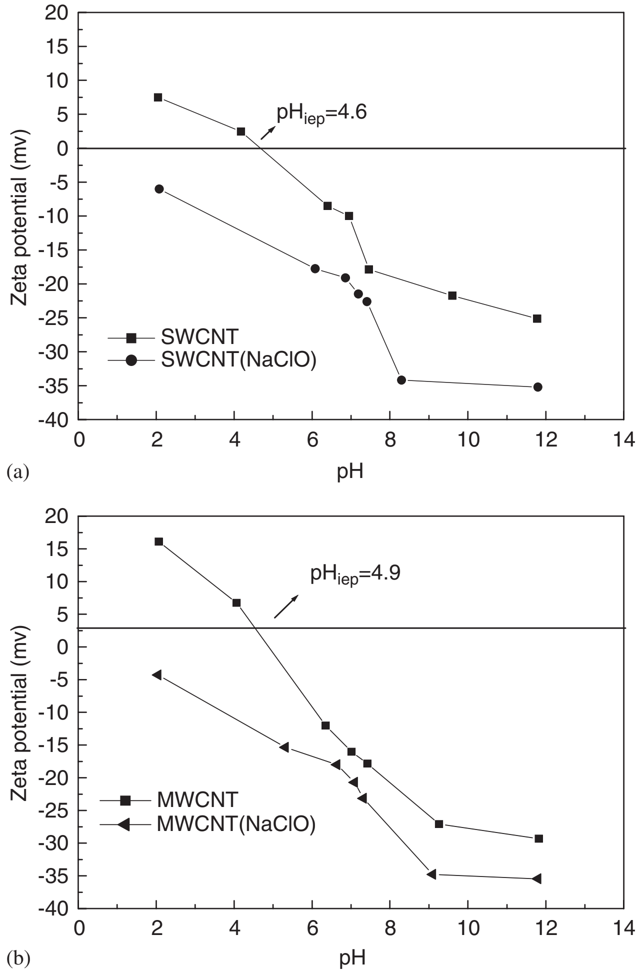

Fig. 7. Effect of pH on the zeta potential of CNTs: (a) SWCNT, (b) MWCNT.

It is also noted that the adsorption capacity of Zn^{2+} with MWCNTs was lower than that with SWCNTs. There are

Table 1
Physical properties of CNTs and PAC

Adsorbent	Surface area ($m^2\,g^{-1}$)	AV pore diameter (nm)	Pore volume ($cm^3\,g^{-1}$)	% Of total pore volume in stated pore size (nm) range		
				2–5	5–10	> 10
SWCNTs	590	7.6	1.12	20.7	29.9	49.4
Purified SWCNTs	423	4.12	0.43	61.6	36.2	2.2
MWCNTs	435	8.35	0.91	17.4	18.2	64.4
Purified MWCNTs	297	5.17	0.38	45.1	29.6	25.3
PAC	852	2.46	0.52	59.7	18.3	22

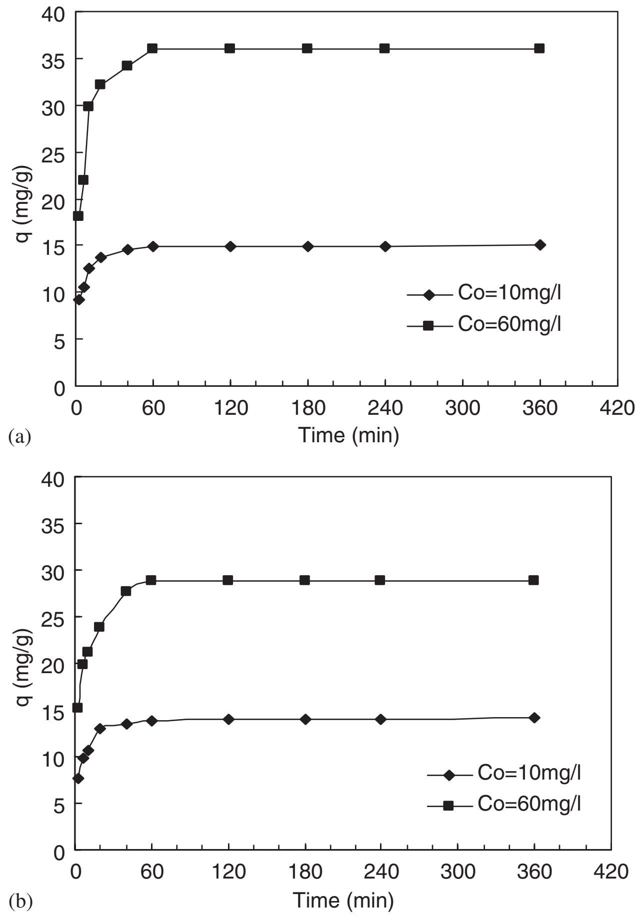

Fig. 8. Effect of contact time on the adsorption of Zn^{2+} with purified CNTs: (a) SWCNT, (b) MWCNT.

two possible reasons to explain the low adsorption capacity of Zn^{2+} with MWCNTs. First, from the BET measurements the surface area and pore volume of purified MWCNTs ($297\,m^2\,g^{-1}$ and $0.38\,cm^3\,g^{-1}$) available for liquid phase mass transfer are lower than those of purified SWCNTs ($423\,m^2\,g^{-1}$ and $0.43\,cm^3\,g^{-1}$). Second, from the Raman spectra the I_D/I_G value of purified MWCNTs (0.371) is higher than that of purified SWCNTs (0.165) indicating that MWCNTs have a larger number of defects present either along the walls of the graphitic tubes or entangled within them. These defects may reduce the effective band overlap, therefore, increase the CNTs' electrical resistivity and lead to a decrease in the adsorption of Zn^{2+} onto CNTs' surface (Tsai and Chen, 2003).

3.3. Adsorption isotherms

Fig. 9 shows the adsorption isotherms of Zn^{2+} with purified SWCNTs and MWCNTs at an initial Zn^{2+} concentration range of $10–80\,mg\,l^{-1}$. As can be seen, the adsorption capacities of Zn^{2+} onto SWCNTs are higher than those onto MWCNTs. The adsorbed amounts of Zn^{2+} onto SWCNTs and MWCNTs were 28.22 and $22.58\,mg\,g^{-1}$, respectively, for $C_e = 10\,mg\,l^{-1}$ and were 39.52 and $30.65\,mg\,g^{-1}$, respectively, for $C_e = 60\,mg\,l^{-1}$.

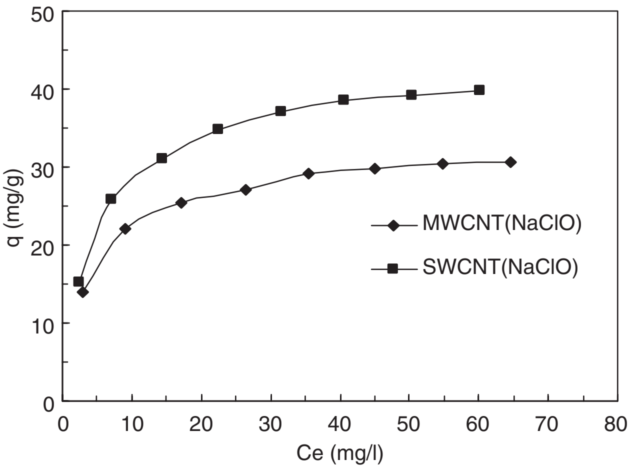

Fig. 9. Adsorption isotherms for Zn^{2+} with purified CNTs.

The constants of Langmuir and Freudlich models are obtained from fitting the adsorption equilibrium data and are listed in Table 2. The correlation coefficients of Langmuir and Freudlich models are 0.999 and 0.945, respectively, indicating that the Langmuir model is more appropriate to describe the adsorption characteristics of Zn^{2+} onto CNTs. The constants a and K_f which are related to adsorption capacity, are higher for adsorption of Zn^{2+} onto SWCNTs, which is consistent with the experimental observation.

3.4. Effect of pH

Figs. 10a and b show the effect of pH on the adsorption of Zn^{2+} onto purified SWCNTs and MWCNTs, respectively. As can be seen, the pH of the solution plays an important role in affecting the adsorption characteristics of Zn^{2+} onto CNTs. With the C_0 of $10\,mg\,l^{-1}$, the adsorption of Zn^{2+} onto CNTs increased with the increase of pH in the pH range of 1–8, fluctuated very little and reached a maximum in the pH range of 8–11 and decreased at a pH of 12. The observation can be explained as follows.

It is known that zinc species can be present in deionized water in the forms of Zn^{2+}, $Zn(OH)^{+1}$, $Zn(OH)_2^0$, $Zn(OH)_3^{-1}$ and $Zn(OH)_4^{2-}$ (Leyva et al., 2002). At $pH < 8$, the predominant zinc species is always Zn^{2+} and the removal of Zn^{2+} is mainly accomplished by adsorption reaction. Therefore, the low Zn^{2+} adsorption that took place at low pH can be attributed in part to competition between H^+ and Zn^{2+} ions on the same sites (Weng and Huang, 2004). Furthermore, the zeta potential of CNTs becomes more negative with the increase of pH as indicated in Fig. 7 which causes electrostatic attraction and thus results in adsorption of more Zn^{2+} onto CNTs. In the pH range of 8–11, the removal of Zn

Table 2
Constants of Langmuir and Freundlich models for adsorption of Zn^{2+} onto purified CNTs and PAC

CNTs	Langmuir			Freundlich		
	a	b	R^2	K_f	n	R^2
SWCNTs	43.66	0.19	0.999	13.24	0.292	0.945
MWCNTs	32.68	0.22	0.999	11.84	0.244	0.945
PAC	13.40	0.07	0.992	3.107	0.309	0.987

Note: Unit: $a = \text{mg}\,\text{g}^{-1}$; $b = \text{mg}^{-1}$; $K_f = 1^n\,\text{mg}^{1-n}\,\text{g}^{-1}$; $n =$ dimensionless; $R =$ dimensionless.

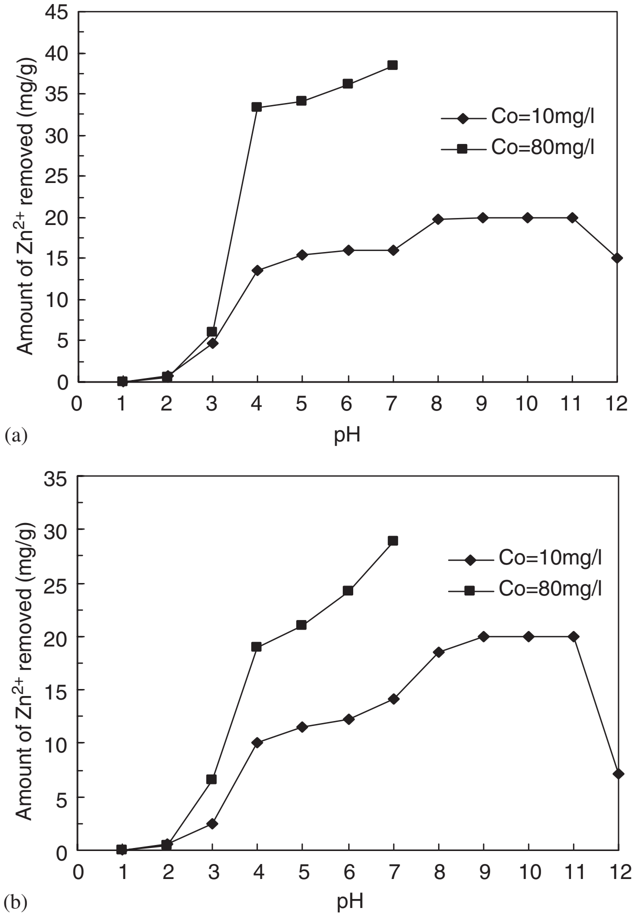

Fig. 10. Effect of pH on the adsorption of Zn^{2+} with purified CNTs: (a) SWCNT, (b) MWCNT.

remained constant and reached maximum. The main species are $Zn(OH)^{+1}$, $Zn(OH)_2^0$ and $Zn(OH)_3^{-1}$ and thus the removal of Zn is possibly accomplished by simultaneous precipitation of $Zn(OH)_{2(s)}$ and adsorption of $Zn(OH)^{+1}$ and $Zn(OH)_3^{-1}$. At a pH of 12, the predominant zinc species are the negative species $Zn(OH)_3^{-1}$ and $Zn(OH)_4^{2-}$ (Leyva et al., 2002). Therefore, the decrease in Zn removal that took place at a pH of 12 can be attributed in part to competition among OH^-, $Zn(OH)_3^{-1}$ and $Zn(OH)_4^{2-}$ ions on the same sites.

With the C_0 of $80\,\text{mg}\,\text{l}^{-1}$, the adsorption of Zn^{2+} onto CNTs increased with the increase of pH in the pH range of 1–7. Above a pH of 7, a large amount of $Zn(OH)_{2(s)}$ was formed and suspended in the solutions.

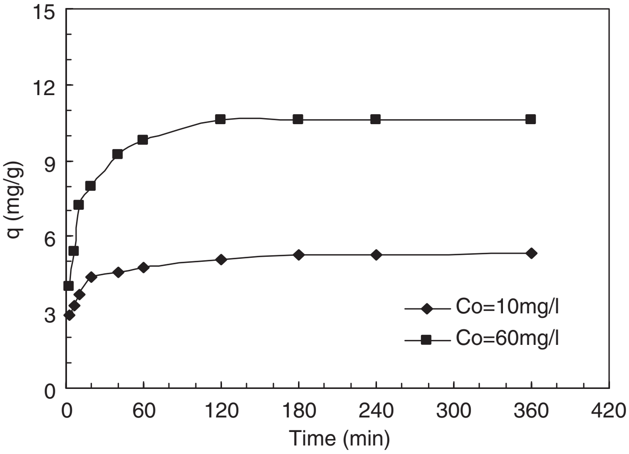

Fig. 11. Effect of contact time on the adsorption of Zn^{2+} with PAC.

3.5. *Comparative study*

In the comparative study, a test for adsorption of Zn^{2+} with commercial PAC (San Ying Enterprises Co., Taipei, Taiwan) was conducted. The surface area, average pore size and pore volume of PAC are also listed in Table 1 and were $852\,\text{m}^2\,\text{g}^{-1}$, 2.46 nm and $0.52\,\text{cm}^3\,\text{g}^{-1}$, respectively. Fig. 11 shows the effect of contact time on the adsorption of Zn^{2+} onto PAC for C_0=10 and $60\,\text{mg}\,\text{l}^{-1}$. It is seen that the contact time to reach equilibrium was 120 min which was longer than the value of 60 min for CNTs. The final adsorption capacities of Zn^{2+} achieved 5.56 and $10.41\,\text{mg}\,\text{g}^{-1}$ for $C_0 =$ 10 and $60\,\text{mg}\,\text{l}^{-1}$, respectively.

Fig. 12 shows the adsorption isotherms of Zn^{2+} onto PAC. It is seen that the adsorbed amounts of Zn^{2+} were 6.34 and $11.12\,\text{mg}\,\text{g}^{-1}$ for $C_e = 10$ and $60\,\text{mg}\,\text{l}^{-1}$, respectively. The constants of Langmuir and Freudlich isotherm models are also listed in Table 2. The correlation coefficients of Langmuir and Freundlich models are 0.992 and 0.987.

By comparing the adsorption characteristics of Zn^{2+} with CNTs and PAC, it is evident that it took less contact time for CNTs to reach equilibrium. This is because the CNTs have no porous structure like PAC in which Zn^{2+} have to move

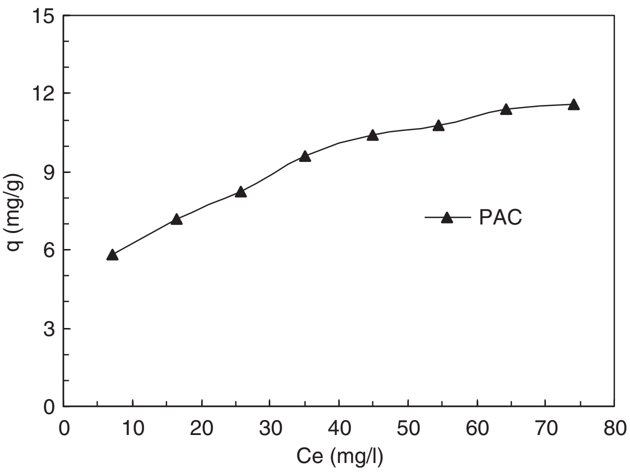

Fig. 12. Adsorption isotherm for Zn^{2+} with PAC.

from the exterior surface to the inner surface of the pores on PAC to reach equilibrium (Peng et al., 2003).

The maximum adsorption capacities of Zn^{2+} calculated by the Langmuir model were 43.66, 32.68, 13.41 $mg\,g^{-1}$ with SWCNTs, MWCNTs and PAC, respectively, at an initial Zn^{2+} concentration range of 10–80 $mg\,l^{-1}$. Although the surface areas of purified SWCNTs (423 $m^2\,g^{-1}$) and MWCNTs (297 $m^2\,g^{-1}$) are much lower than that of PAC (852 $m^2\,g^{-1}$), the adsorption capacities of Zn^{2+} onto purified SWCNTs and MWCNTs are much higher than that onto PAC. This is due to the fact that oxidation of carbon surface can provide not only a more hydrophilic surface structure but also many oxygen-containing groups, which increase the ion-exchange capacity of carbon materials (Li et al., 2003a), therefore, lead to a significant increase in the adsorption of Zn^{2+} onto CNTs. The short time needed to reach equilibrium as well as the high adsorption capacity of Zn^{2+} suggests that purified SWCNTs and MWCNTs have great potential applications for the removal of zinc from water.

4. Conclusions

The following conclusions could be drawn from this study:

1. The properties of CNTs such as purity, structure and nature of the surface are greatly improved after purification by sodium hypochlorite solutions which made CNTs become more hydrophilic and suitable for adsorption of Zn^{2+} from water.
2. In general, the adsorption of Zn^{2+} onto CNTs increases with the increase of pH in the pH range of 1–8, fluctuates very little and reaches a maximum in the pH range of 8–11 and decreases at a pH of 12.
3. The contact times to reach equilibrium are 60 min for SWCNTs and MWCNTs and 120 min for PAC.
4. The maximum adsorption capacities of Zn^{2+} calculated by the Langmuir model are 43.66, 32.68, 13.41 $mg\,g^{-1}$ with SWCNTs, MWCNTs and PAC, respectively, at an initial Zn^{2+} concentration range of 10–80 $mg\,l^{-1}$.
5. The short time needed to reach equilibrium as well as the high adsorption capacity of Zn^{2+} as compared to commercial PAC suggests that SWCNTs and MWCNTs possess highly potential applications for the removal of Zn^{2+} from water.

Acknowledgements

Support from the National Science Council, Taiwan, under Contract no. NSC 93-2211-E-005-020 is gratefully acknowledged.

References

Dresselhaus, M.S., Dresselhaus, G., Jorio, A., Souza Filho, A.G., Saito, R., 2002. Raman spectroscopy on isolated single wall carbon nanotubes. Carbon 40, 2043–2061.

Eckenfelder, W.W., 1989. Industrial Water Pollution Control. McGraw-Hill International Edition, Singapore.

Ko, C.J., Lee, C.Y., Ko, F.H., Chen, H.L., Chu, T.C., 2004. Highly efficient microwave-assisted purification of multiwalled carbon nanotubes. Microelectronic Engineering 73–74, 570–577.

Leyva, R.R., Bernal, J.L.A., Mendoza, B.J., Fuentes, R.L., Guerrero, C.R.M., 2002. Adsorption of zinc(II) from an aqueous solution onto activated carbon. Journal of Hazardous Materials B90, 27–38.

Li, Y.H., Wang, S., Wei, J., Zhang, X., Xu, C., Luan, Z., Wu, D., Wei, B., 2002a. Lead adsorption on carbon nanotubes. Chemical Physics Letters 357, 263–266.

Li, Y.H., Xu, C., Wei, B., Zhang, X., Zheng, M., Wu, D., Ajayan, P.M., 2002b. Self-organized ribbons of aligned carbon nanotubes. Chemical Materials 14, 483–485.

Li, Y.H., Wang, S., Luan, Z., Ding, J., Xu, C., Wu, D., 2003a. Adsorption of cadmium(II) from aqueous solution by surface oxidized carbon nanotubes. Carbon 41, 1057–1062.

Li, Y.H., Wang, S., Wei, J., Zhang, X., Wei, J., Xu, C., Luan, Z., Wu, D., 2003b. Adsorption of fluoride from water by aligned carbon nanotubes. Material Research Bulletin 38, 469–476.

Long, R.Q., Yang, R.T., 2001. Carbon nanotubes as superior sorbent for dioxin removal. Journal American Chemical Society 123, 2058–2059.

Lu, C., Chung, Y.L., Chang, K.F., 2005. Adsorption of trihalomethanes from water with carbon nanotubes. Water Research 39, 1183–1189.

Peng, X., Li, Y., Luan, Z., Di, Z., Wang, H., Tian, B., Jia, Z., 2003. Adsorption of 1,2-dichlorobenzene from water to carbon nanotubes. Chemical Physics Letters 376, 154–158.

Purdom, P.W., 1980. Environmental Health. Academic Press, New York.

Tsai, C.L., Chen, C.F., 2003. Characterization of bias-controlled carbon nanotubes. Diamond and Related Materials 12, 1615–1620.

Weng, C.H., Huang, C.P., 2004. Adsorption characteristics of Zn(II) from dilute aqueous solution by fly ash. Colloids and Surfaces A: Physicochemical Engineering Aspects 247, 137–143.

Yang, Q.H., Hou, P.X., Bai, S., Wang, M.Z., Cheng, H.M., 2001. Adsorption and capillarity of nitrogen in aggregated multi-walled carbon nanotubes. Chemical Physics Letters 345, 18–24.